STUDY OF TURBULENT TRAILING-EDGE FLOW USING DIRECT NUMERICAL SIMULATION[1]

Yufeng Yao and Neil D. Sandham
Department of Aeronautics & Astronautics, University of Southampton
Highfield, Southampton SO17 1BJ, UK

Trevor G. Thomas and John J.R. Williams
Department of Engineering, Queen Mary & Westfield College
Mile End Road, London E1 4NS, UK

ABSTRACT

This paper presents a direct numerical simulation (DNS) of turbulent flow over a rectangular trailing edge geometry at a Reynolds number of 1000 based on the trailing edge thickness. The study is carried out first with a turbulent boundary layer flow calculation, producing time-dependent data for the inflow condition, followed by the turbulent trailing edge flow simulation. A parallel simulation code is used, which is based on a finite difference scheme and a multi-grid Poisson solver. The computed flow has been studied for the effects of domain size and grid resolution. Comparison of the mean quantities and turbulence statistics has been made. The characteristics of vortex shedding are revealed by the time history of lift and pitching moment and their power spectra, from which the main shedding frequency (nondimensionally equal to 0.1) is clearly shown together with other harmonic frequencies. A series of instantaneous flow structures in a shedding period is visualized, providing further understanding of the shedding dynamics and the interaction between the pressure field and vortices in the near wake region. A high-resolution simulation with a total of $256 \times 512 \times 64$ grid points in the computational domain is carried out to analyse the energy budget in both the boundary layer and wake regions.

INTRODUCTION

The turbulent flow behind a rectangular trailing-edge geometry has always presented a difficulty to fluid flow researchers, because the sudden removal of the solid wall initiates an interaction between two separate turbulent boundary layers in the near-wake region. The turbulence models traditionally used by the computational fluid dynamics (CFD) community are challenged in such a region, where the fluid is in a non-equilibrium state. Hence more precise methods such as direct numerical simulation (DNS) are required to provide more insight.

[1] This work has been supported by the UK Engineering and Physical Science Research Council (EPSRC) through the financial and parallel computer grants GR/L 18570 and GR/M 08424.

Experimental and numerical studies have been conducted recently to investigate the trailing edge flow problem. Gough and Hancock (1996) carried out an experimental study with two symmetric incoming turbulent boundary layers (each with δ_{99} at the trailing edge end equal to 10 times the trailing edge thickness h) and a Reynolds number (based on the boundary layer momentum thickness θ) of 600. For this configuration it was found that a mean recirculation region existed behind the trailing edge and a coherent von Kármán vortex street appeared in the near wake up to about $10h$, beyond which it was mostly scrambled by the presence of small scale turbulence. The same flow was investigated computationally by Gao et al. (1996) using the large eddy simulation (LES) technique. They produced reasonable qualitative agreement with the experiments for various turbulence statistics but quantitative differences existed, which were attributed to the differences in the inflow boundary layers. It is believed that the upstream incoming flow has a significant influence on the downstream flow field, and therefore an accurate simulation of the inflow turbulent boundary layer is a necessary requirement for performing an accurate trailing edge flow simulation.

The overall arrangement of the present simulation is shown in figure 1; here, a boundary layer (precursor) simulation is used to generate the inflow data for the following trailing edge (successor) simulation, and is arranged so that the Reynolds number Re_h (based free stream velocity U_e and plate thickness h) is equal to 1000. The simulated flow is investigated to assess the effects of domain size and grid resolution and is then used to study the characteristics of of the vortex shedding and to determine the turbulence kinetic energy budgets. Finally, flow visualisation is used to reveal the geometrical structure of the flow.

NUMERICAL METHOD AND SIMULATIONS

The Navier-Stokes equations are discretized on a staggered grid using second order finite differences, and advanced in time by the projection method based on the second order Adams-Bashforth scheme. The provisional velocity is projected using the data

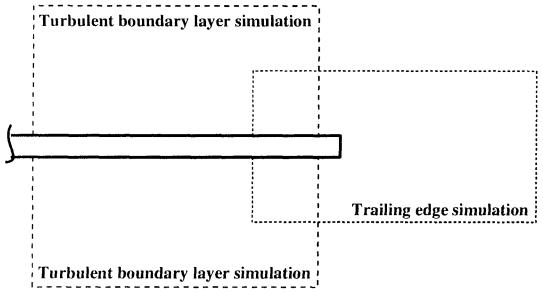

Figure 1: Definition sketch showing the arrangement of the turbulent boundary layer and trailing edge simulations.

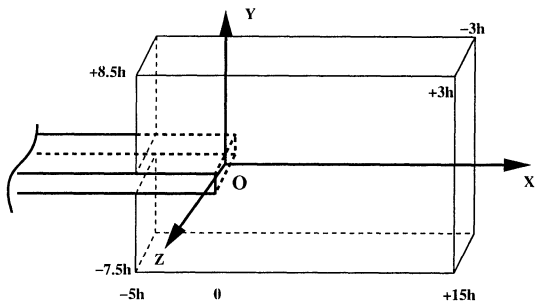

Figure 2: Computational box for trailing edge flow simulation.

from the current time step. The velocity at the new time step is corrected based on the pressure, which is obtained by the solution of a Poisson equation, to satisfy continuity.

The complete simulation has two separate parts. The boundary layer calculation runs first, followed by the trailing edge simulation. The turbulent boundary layer flow is computed using a spatial DNS code, which has been adapted from a temporal channel flow DNS code (Sandham, 1994). The spatial development breaks the streamwise periodicity and the technique of Lund et al. (1998) is used to re-scale the turbulence from near the outflow and feed it back as the inflow condition. The method has been validated with laminar and turbulent boundary layer flows and results compare well with experiment and other simulations (Yao et al., 1999). A time sequence of flow variables at one plane is stored for later use as the inflow boundary condition in the trailing edge flow simulation. The trailing edge flow simulation is carried out with a recently-developed complex-geometry code which uses the same finite difference scheme described above with a multi-grid Poisson solver. The code is parallelized based on the concept of constructing the computational domain with an assembly of rectangular blocks with their faces mapped either to each other or to boundary conditions. It is implemented in C/C++ and uses MPI parallel message libraries. A parallel multigrid algorithm is used for solving the Poisson equation, details of which can be found in Thomas and Williams (1997). The code has been validated for different cases such as the backward facing step flow, open channel flow, and flow over a ground-mounted cube, all giving good agreement with published computational and experimental data.

The boundary conditions are defined as follows. At the inlet plane the inflow data from the boundary layer simulation are made available by a 'slice server' device. The upper and lower parts of the inflow are taken from a single simulation, and are thus statistically identical, but with sufficiently large lag to be uncorrelated in time. The outlet boundary conditions are treated with a convective condition, so that outgoing disturbances leave the domain smoothly. On the upper and lower surfaces free-slip conditions are used and in the spanwise direction a periodic condition is adopted.

RESULTS AND DISCUSSION

The definition of the computational box for the trailing edge simulation is shown on figure 2. The origin of the coordinate system is located at the centre of the trailing edge end plane. A baseline simulation (case A) is set up with a box of $20h \times 16h \times 6h$ in the streamwise (x), wall-normal (y) and spanwise (z) directions respectively. The length in the streamwise direction L_x includes the $5h$ trailing edge plate and $15h$ wake region for the development of the incoming turbulent boundary layer and the wake. The computational domain extends some distance up-stream of the trailing edge, thus permitting the up-stream boundary layer flow to be influenced by the motions in the down-stream wake flow. Hence it is possible to follow the natural progress from a boundary-layer flow to a wake flow. In the wall-normal direction the box length (L_y) is $16h$, with $8.5h$ in the upper and $7.5h$ in the lower part of the wake. Compared to the inflow turbulent boundary layer thickness δ_{99}, which is $6.42h$ in the present simulation, the length is large enough to develop the incoming boundary layer along the trailing edge plate. The spanwise length (L_z) is $6h$, the same as that in the turbulent boundary layer simulation. The computational domain is decomposed in three directions, resulting in 256 blocks with 4 blocks along the trailing-edge geometry and 252 blocks in the flow field. The grid points are uniformly distributed with a grid of $128 \times 256 \times 64$. In each block there are $32 \times 16 \times 16$ grid points and a 5 level multi-grid sequence can be constructed. The simulations are carried out on a Cray T3E-1200 parallel computer.

The general features of the wake development can be determined from the mean flow field. The case A simulation shows that a recirculation region exists; this extends to a point about $2h$ downstream of trailing edge and has a maximum reverse velocity of about 10% of the free-stream velocity (U_e). The mean velocity U recovers to 50% of U_e at about $10h$ downstream of the trailing edge and 55% of U_e near the outlet plane.

The effect of the domain size and grid resolution on the computational results has been studied further with an additional five cases, namely case B: with a 50% longer box in the streamwise direction; case C: with a 50% wider box in the wall-normal direction; case D: with double the number of grid points in the streamwise direction; case E: with double the number of grid points in the wall-normal direction; and case F: with double the num-

Case	Domain Size	Domain Grids
A	$20h \times 16h \times 6h$	$128 \times 256 \times 64$
B	$30h \times 16h \times 6h$	$192 \times 256 \times 64$
C	$20h \times 24h \times 6h$	$128 \times 384 \times 64$
D	$20h \times 16h \times 6h$	$256 \times 256 \times 64$
E	$20h \times 16h \times 6h$	$128 \times 512 \times 64$
F	$20h \times 16h \times 6h$	$128 \times 256 \times 128$

Table 1: The effects of domain size and grid resolution.

ber of grid points in the spanwise direction (see table 1). A detailed comparison can be found in Yao et al. (1999). Here only the essential results and conclusions are given. The domain size change (cases B and C) does not produce any obvious effects on the main features of the boundary layer and wake development. The basic arrangement (case A) is concluded to be sufficiently large for the present trailing edge simulation and can be used further for grid resolution studies. In the grid resolution studies the grid refinement has only a minor effect on the boundary-layer flow along the trailing edge plate in both the streamwise and spanwise directions (cases D and F). Thus the case A simulation has been well resolved in these directions. However grid refinement does have an effect in the wall-normal direction (case E), where a higher peak turbulent kinetic energy is detected. Downstream in the wake region the maximum difference occurs in the recirculation region and gradually diminishes in the far-wake region.

To analyse the grid resolution in the boundary layer region the grid spacing in wall units has been computed, resulting in $\Delta x^+ = 7.81$, $\Delta y^+(1) = 3.13$ and $\Delta z^+ = 4.69$ at the inlet plane of case A. Comparing with Spalart and Leonard (1985) (who used a spectral method and $\Delta x^+ = 13$, $\Delta z^+ = 6.5$) the current simulation (with a finite difference method) has about 70% and 40% more grid points in the x and z directions respectively. With such a factor of extra points the results from the simulation are expected to be comparable based on our previous experience of channel flow. Obviously the flow in the wall-normal direction is not resolved as there are only three points in the sublayer region. Doubling the points (in case E) does improve the grid resolution in the y-direction. In the wake region the grid resolution is represented in wake units as $\Delta\tilde{x}_i = \Delta x_i \delta U_m/\nu$, where the δU_m is mean velocity deficit and Δx_i is the grid spacing. Comparing against the plane far-wake DNS of Moser et al. (1998), in which $\Delta\tilde{x} = 97.66$ and $\Delta\tilde{y} = 82.05$, we have (in case A) $\Delta\tilde{x} = 167$ and $\Delta\tilde{y} = 67$ at locations in the recirculation region. It can be seen that case A is not quite as well resolved in the streamwise direction. However, in the wall-normal (y) direction the flow is over-resolved in comparison to Moser et al.'s simulation due to the very strict requirement for the boundary-layer resolution. Based on the discussion of grid resolution above it was felt necessary to carry out further simulation in which the flow is well resolved in all three directions. A high-resolution simulation (case G) has been carried out with a total of $256 \times 512 \times 64$ grid points.

The vortex shedding behaviour at the trailing edge is characterized by its shedding frequency f_0 (or Strouhal number $S_t \equiv f_0 h/U_e$), and this can be deduced from the variation of the force coefficients on the plate over time. Figure 3 gives the time history of lift (F_y) and pitching moment (M_z) about axis z from which the period can be estimated by measuring the gap between neighbouring peak positions. The period is about $10h/U_e$, and hence the main vortex shedding occurs at a Strouhal number S_t of about 0.1. This result can be confirmed by looking at the power spectra over a time record of 180 time units (see figure 4). Both show that the largest peak value appears at the position where the main frequency (f_0) equals to $0.1U_e/h$. Also the harmonic shedding frequencies (f_1 and f_2) and the sub-harmonic shedding frequencies ($f_{1/2}$ and $f_{1/4}$) are observed in the responses.

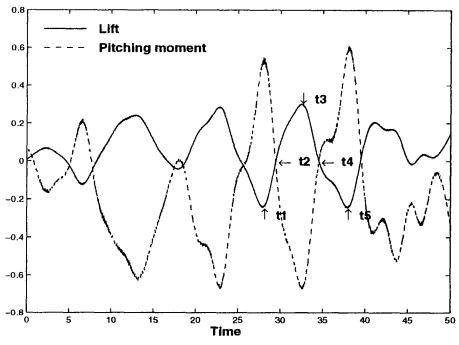

Figure 3: Time history of the lift and pitching moment.

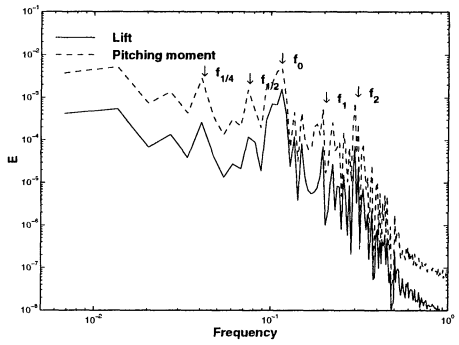

Figure 4: Power spectra of the lift and pitching moment over a time interval of $180h/U_e$.

It is also interesting to visualize instantaneous flow structures in the near wake region as these reveal the geometric structure of the flow. Starting from a time position (corresponding to the time t_1 in figure 3), a series of five instantaneous snapshots of the flow (from case G simulation) are shown on figure 5(a–f). These illustrate how the flow changes with time, and how the axial vorticity present in the inflow becomes wrapped around the rotating low pressure tubes (von Kármán billows). The interaction between these low pressure tubes (presented in darker colour, a surface of constant pressure) and the strained axial vortices (presented in light colour, a surface of constant negative second invariant

of velocity gradient) is shown quite clearly. Such an interaction was discussed in Yao et al. (1999) and a brief description is given as follows. The pressure tubes are shed from the trailing-edge as quasi two-dimensional structures and arrange themselves in a staggered manner similar to the von Kármán (VK) vortex street. They rotate clock-wise on the upper side and anti-clockwise on the lower side with the same sign vorticity as their originating boundary layers. The incoming axial vortices, which are an inherent part of the boundary layer flow, are strained and deformed when they encounter these pressure tubes; the maximum staining occurs at the location of the (free) stagnation points positioned between successive pressure tubes, and the axial vortices are enhanced along the direction of maximum stretch. At the same time the pressure tubes are perturbed and eventually destroyed by the strengthened vortices.

An energy budget analysis can be made based on the turbulence kinetic energy equation

$$\frac{\partial k}{\partial t} + \langle u_i \rangle \frac{\partial k}{\partial x_i} = P_r - \epsilon - \frac{\partial (J_i^u + J_i^p + J_i^\nu)}{\partial x_i}, \qquad (1)$$

where $\langle u_i \rangle \frac{\partial k}{\partial x_i}$ is the convection term, P_r is the production term, ϵ is the dissipation and J_i^u, J_i^p, J_i^ν are turbulence triple-moment, pressure and viscous flux terms, respectively. The turbulence kinetic energy budgets are given in figure 6(a–f).

In the boundary layer region alongside the plate (figure 6a–b) the dominant term in the energy balance is the production term; this takes its maximum value at about $y^+ \sim 10$. Closer to the plate, $y^+ < 10$, the viscous flux term dominates. The dissipation term remains the largest energy drain over the whole thickness of the boundary layer, and outside the buffer layer, $y^+ > 25$, the balance is (mostly) between the production and dissipation terms, so that $P_r \sim \epsilon$ approximately. The overall energy balance indicated by the residual error in the summation appears to be quite small.

In the recirculation region just downstream of the trailing edge (figure 6c) the production has a negative peak in the reverse flow area and a positive peak away from the central region. Comparing (c) with (a) or (b) it can be seen that the convection term and the pressure flux term grow rapidly and reach higher values than the production term. In contrast, the viscous flux term approaches zero due to the absence of the solid wall. At the end of the recirculation region, (figure 6d), the production has increased and exceeds the magnitudes of other terms, and becomes largest term in the budget. In the middle of the recirculation region (figure 6c) the energy balance is dominated by the convective transport, pressure flux, and production terms. Further downstream, outside of the recirculation region, the triple-moment flux term has increased to become the largest individual term. Also, the pressure flux term in the central part of the wake appears to change sign when moving from points inside the recirculation zone to points further downstream in the developing wake. Further downstream (figure 6,e–f) all terms are decreasing, although the convection term becomes relatively more significant. Overall good budget balances are achieved.

CONCLUSIONS

It can be concluded from this research that the DNS technique is feasible for the simulation of the turbulent flow over a rectangular trailing-edge geometry at a Reynolds number $Re_h = 1000$. The mean flow features have been determined together with turbulence statistics and turbulence kinetic energy budgets. The computed flow has been tested for the effects of domain size and grid resolution. A comparison of the mean quantities and turbulence statistics has been made. The characteristic frequency of the vortex shedding, as determined from the history of the lift and pitching moments, and from the power spectra, corresponds to a Strouhal number of 0.1, and other harmonic components are also present. The complicated flow structure and the interaction between the axial components of vorticity , present in the plate boundary layer, and the von Kármán billows, produced by the unsteady wake dynamics, have been investigated using three-dimensional visualization, including snapshots taken at different times within a shedding cycle. These provide a clear insight into the geometry of the flow. A high-resolution simulation with a total of $256 \times 512 \times 64$ grid points is carried out and good balance of energy budgets has been achieved.

References

Gao, S.A., Voke, P.R., and Gough, T.D. 1996, Turbulent Simulation of a Flat Plate Boundary Layer and Near Wake, *Proceedings, 2nd ERCOFTAC Workshop on Direct and Large Eddy Simulation,* Vol. 1.

Gough, T.D. and Hancock, P.E. 1996, Lower Reynolds Number Turbulent Near Wakes, *Advances in Turbulence VI,* S. Gavrilakis et al., ed., pp. 445-448.

Lund, T.S., Wu, X., and Squires, K.D. 1998, Generation of Turbulent Inflow Conditions for Spatially Developing Boundary Layer Simulations, *J. Computational Physics,* **140**(2), pp. 233-258.

Moser, R.D., Rogers, M.M., and Ewing, D.W. 1998, Self-similarity of Time-evolving Plane Wakes, *J. Fluid Mech.*, **367**, pp. 255-289.

Spalart, P.R. and Leonard, A. 1985, Direct Numerical Simulation of Equilibrium Turbulent Boundary Layers, *Proceedings, 5th Symp. on Turbulent Shear Flows*, Ithaca, NY, pp. 234-252.

Sandham, N.D. 1994, Resolution Requirement for Direct Numerical Simulation of Near Wall Turbulent Flow using Finite Difference, *QMW-EP-1097,* Dept. of Engineering, Queen Mary & Westfield College, University of London.

Thomas, T.G. and Williams, J.J.R. 1997, Development of a Parallel Code to Simulation Skewed Flow over a Bluff Body, *J. of Wind Engineering and Industrial Aerodynamics,* **67&68**, pp. 155-167.

Yao, Y.F., Thomas, T.G., Sandham, N.D. and Williams, J.J.R. 1999, Direct Numerical Simulation of Turbulent Flow over a Rectangular Trailing Edge, submitted to *Theoretical and Computational Fluid Dynamics.*

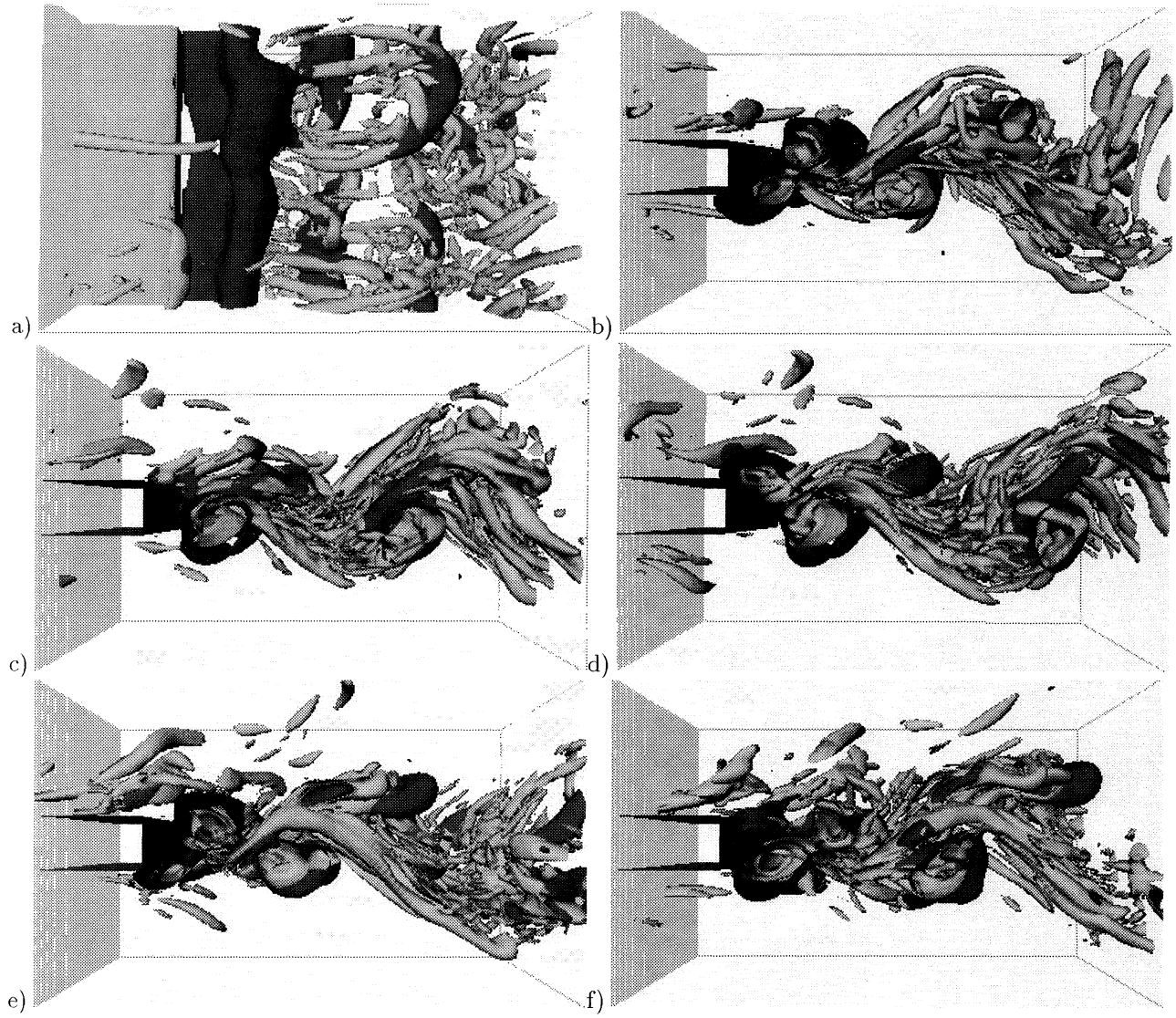

Figure 5: Instantaneous flow structure in the near wake region (darker colour: pressure tube; light colour: vortices). a) a top view at time t_1, b) a side view at time t_1, c) a side view at time t_2, d) a side view at time t_3, e) a side view at time t_4, f) a side view at time t_5. Times t_1, t_2, t_3, t_4, t_5 are shown on figure 3.

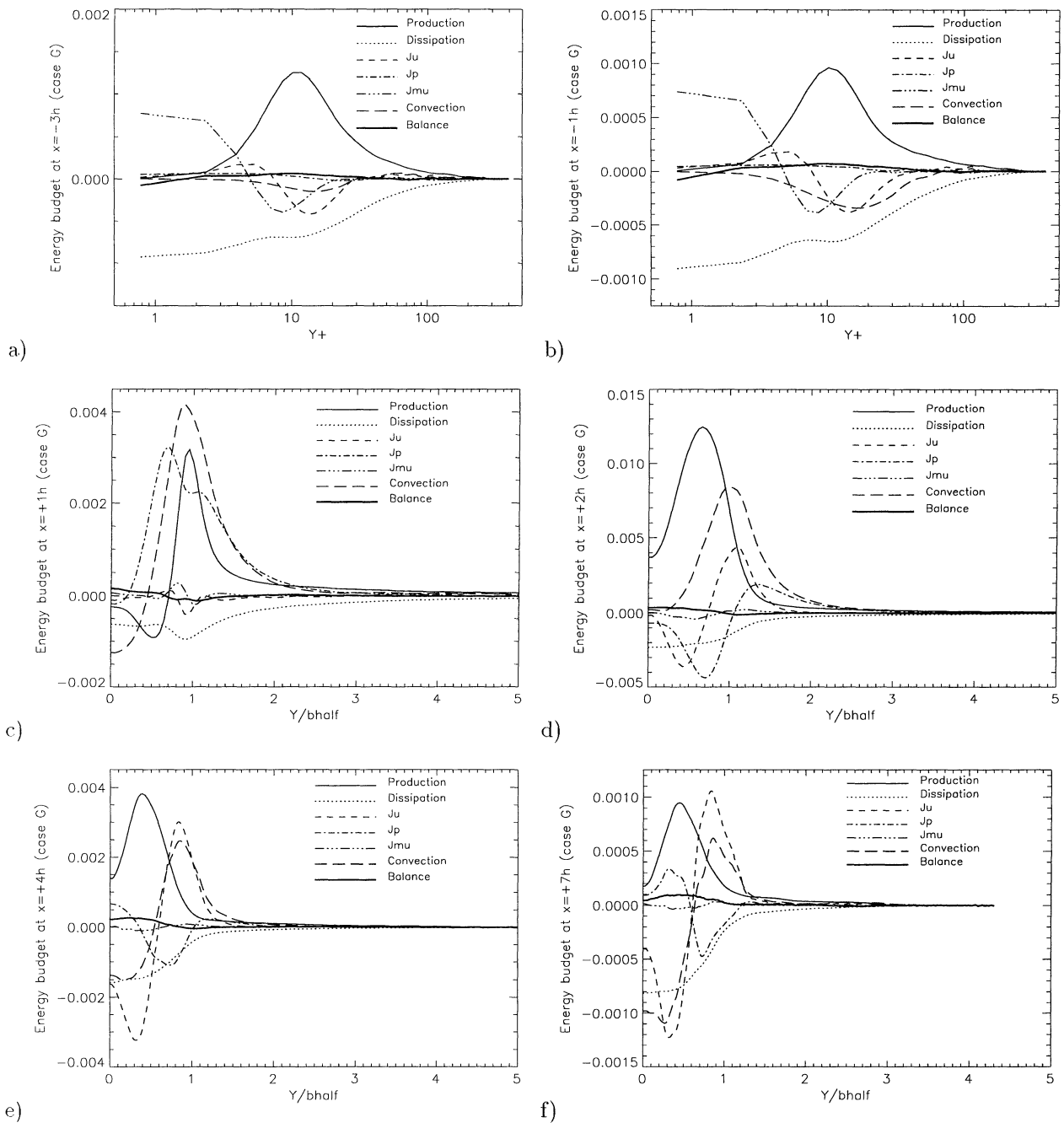

Figure 6: Energy budgets at six streamwise stations in the trailing edge flow simulation. a) at $x = -3h$ in the turbulent boundary layer region, b) at $x = -1h$ in the turbulent boundary layer region, c) at $x = +1h$ in the near wake region, d) at $x = +2h$ in the near wake region, e) at $x = +4h$ in the near wake region, f) at $x = +7h$ in the far wake region.